Single-Image Vignetting Correction by Constrained Minimization of log-Intensity Entropy

Torsten Rohlfing

***Abstract*—Vignetting is the lateral intensity drop-off observed in photographic images due to optical properties of the lens system. In digital photography, directional sensitivity profiles of camera sensors add further to this effect. This paper introduces a new method for calibration-free retrospective correction of vignetting in a single image and makes two original contributions: firstly, we apply the concept of information minimization to vignetting correction using log-intensity entropy as a scaling-invariant information measure with superior convergence properties for intensity artifact correction. Second, a constrained radial polynomial vignetting function ensures monotonic intensity profiles. The resulting devignetting algorithm is computationally highly efficient and robust without requiring any image segmentation, which we demonstrate using realistic synthetic ground truth data. Compared with a state-of-the art technique, we show that our method performs up to an order of magnitude faster while producing more accurate results. Our method is also substantially more robust to using downsampled image data. Finally, because the radial vignetting parametrization and the entropy criterion are completely independent, our method can also correct non-radial exposure effects.**

***Index Terms*—single-image vignetting correction; information minimization; log-intensity entropy; constrained parameterization**

I. Introduction

VIGNETTING is the lateral intensity drop-off observed in photographic images. According to their cause, three types of vignetting are usually considered [1]: natural vignetting, pixel vignetting, and mechanical vignetting. Natural vignetting, which affects digital and film cameras alike, is an optical effect due to the properties of the lens system. Pixel vignetting, which affects only digital cameras, is a result of angle-dependent sensitivity of the image sensor. Mechanical vignetting is a result of occlusion by objects entering the camera field of view, such as an oversized lens hood. For the purpose of this paper, like the vast majority of works in the field, we limit our consideration to the correction of the gradual and continuous natural and pixel vignetting.

Vignetting is immediately apparent when multiple images taken of the same scene at different angles are stitched into a single, panoramic image (i.e., mosaicing). When the periphery (where darkening is strong) of one image overlaps the center (where there is no darkening) of the neighboring image, the relative intensity differences become obvious. The vast majority of devignetting algorithms [2], [3], [4] thus work on multiple overlapping images. This simplifies the devignetting problem, because by comparing intensities of the corresponding pixels from multiple images, the drop-off function can be estimated and corrected. These methods cannot be applied, however, when only a single image is available or when image overlap is insufficient.

Using only a single image, vignetting can be *prospectively* corrected by introducing a calibration stage, i.e., for a given lens system and aperture (and, for zoom lenses, a given focal length) a flat white, uniformly illuminated surface is first photographed. From the spatial intensity distribution of this calibration exposure the vignetting function is then computed at each pixel [5], [6]. By contrast, the devignetting algorithm presented herein works on a single picture, but does so *retrospectively*, i.e., it does not require any calibration.

To the best of our knowledge, there are currently only two other retrospective single-image devignetting methods that have been applied to photographic images. The first, by Zheng *et al.* [7], segments the image into regions and then fits vignetting functions to the image intensities within these regions. The second, also by Zheng *et al.* [8], which does not involve segmentation, is a technique based on the observed symmetry of radial gradient distributions in natural images.

For microscopy images, Leong *et al.* [9] describe a method for vignetting correction that is based on smoothing the entire image with a Gaussian kernel to eliminate image structure and retain only the low-frequency intensity vignetting field. The method has an adjustable parameter, the kernel size, that depends on image content (i.e., the scale of objects in the image), sampling parameters (i.e., image size), and optical system properties (i.e., the spatial variation of the vignetting function). We furthermore observe that microscopy images typically consist of a single global image region, whereas photographic images usually contain several, in the simplest case foreground vs. background, which suggests that a simple global smoothing operation is likely not sufficient to estimate and correct vignetting in photographies.

The new devignetting technique introduced herein is based on a method developed by Likar *et al.* [10], who demonstrated that image entropy is a suitable optimization criterion for the model-free correction of shading artifacts, also initially for microscopy image shading correction. The underlying assumption of the method is that, absent photometric artifacts, homogeneous objects should be imaged with homogeneous intensity, corresponding to a sharp histogram with a single peak and low entropy. A spatially varying intensity bias field, such as vignetting, would then spread this peak, thus introducing additional information content and raising entropy. The task of correcting the bias field is, therefore, equivalent

*T. Rohlfing is with the Neuroscience Program at SRI International, 333 Ravenswood Avenue, Menlo Park, CA 94025-3493, USA. Phone: +1-650-859-3379, fax: +1-650-859-2743 (e-mail: torsten@synapse.sri.com).

to undoing this effect by minimizing image entropy.

The key contributions of our paper are: a) the derivation of log-intensity entropy as a scale-invariant measure of image information, b) the application of log-intensity entropy minimization to devignetting, and c) a constrained monotonic radial polynomial parametrization of the drop-off function. Compared with [7], our method does not require any image segmentation, which makes it substantially simpler (indeed almost trivial) to implement. It is also computationally efficient, and perhaps more universal, as it does not depend on color (i.e., it works equally well on black-and-white images) or require the presence of any segmentable objects in the imaged scene. Compared with [8], we demonstrate herein that our method is faster by an order of magnitude, yet produces more accurate results and is more robust to downsampled images. Finally, our method completely separates the vignetting parametrization from the figure of merit used for optimization. Our method is, therefore, equally applicable to effects that are non-radial.

II. Methods

The devignetting method introduced herein comprises three key components, each of which is described in one of the following subsections. The first is a log-intensity entropy criterion for vignetting correction, and the second is a constrained monotonic parametrization of the vignetting function. The third component is an optimization algorithm that finds the parameters of the vignetting model which minimize the log-intensity entropy of the corrected image.

Vignetting is essentially independent of color, i.e., the red, green, and blue channels of a pixel in an RGB image are all affected by the same darkening, and to correct vignetting all channels must be multiplied by the same correction factor. Consideration can, therefore, be limited to the correction of gray-level images. To obtain a gray-level image from a color image, we specifically implemented the following conversion from RGB to luminance:

$$L = 0.2126 \cdot R + 0.7152 \cdot G + 0.0722 \cdot B. \tag{1}$$

In our experience, other weightings (for example $1/3(R+G+B)$) essentially produce the same devignetting results.

A. Log-Intensity Entropy Criterion

Minimization of image entropy has been previously used as a method for correction of shading artifacts [10]. While somewhat effective, this criterion suffers from a fundamental limitation, which we explore below, as it encourages local optima in the optimization.

Formally, let X be a probability distribution (here: a distribution on image intensities) with probability density function f. Then the differential entropy h_X of X is

$$h_X = -\int_{\mathbb{X}} f(x) \log f(x)\, dx. \tag{2}$$

If X is scaled by a non-zero factor c, then the differential entropy of the scaled distribution (c.f., [11]) is

$$h_{cX} = h_X + \ln|c|. \tag{3}$$

Thus, in the case of image intensities that are brightened by a factor $c > 1$ to correct for vignetting, $\ln|c| > 0$ and the entropy increases. This counteracts the reductions in overall entropy that arise from improved overlap between intensity distributions at different radii, which leads to undesirable local optima in the minimum entropy criterion (see entropy values vs. distribution shift in Fig. 1). Entropy is, however, shift invariant, i.e.,

$$h_{c+X} = h_X, \tag{4}$$

which can be exploited via

$$h_{\ln cX} = h_{\ln c + \ln X} = h_{\ln X} \tag{5}$$

to identify the *entropy of the log-intensity image* as a scaling-invariant devignetting criterion. Note that this is fundamentally different from simply log-transforming the data to make the intensity correction additive, rather than multiplicative, as has been proposed by others [12].

B. Discrete Entropy Estimation

Entropy computation for discrete distributions is non-trivial [13] and easily biased. Following Likar *et al.* [10], we implemented an approach using discrete histograms. First, the luminance values L, which range from 0 to 255 for 8-bit images, are mapped to N histogram bins i as follows:

$$i(L) = (N-1)\log(1+L)/\log 256. \tag{6}$$

The histogram bins n_k are then populated from the luminance values L over all pixels (x, y):

$$\begin{aligned} n_k = &\sum_{\substack{x,y:\\ \lfloor i(L(x,y))\rfloor = k}} (1 + k - i(L(x,y))) \\ &+ \sum_{\substack{x,y:\\ \lceil i(L(x,y))\rceil = k}} (k - i(L(x,y))) \end{aligned} \tag{7}$$

This double sum is just a complicated way of expressing that samples between two histogram bins are distributed with linear weights across these two bins.

It is possible that, due to local intensity increases applied by devignetting, the corrected image intensity range exceeds 255. In this case the algorithm simply adds histogram bins at the upper end without rescaling the distribution, and the sum in Eq. 9 is extended accordingly. This maintains consistency of entropy evaluations and avoids pile up of samples in the highest histogram bin, which would otherwise lead to biased estimates.

To account for gaps in the image intensity distribution that can arise when scaling quantized data, the histograms are then smoothed using a Gaussian kernel, G_σ, with standard deviation σ:

$$\hat{\mathbf{n}} = \mathbf{n} * G_\sigma. \tag{8}$$

Especially for large kernel sizes, this two-stage strategy of histogram creation and smoothing is far more efficient than directly entering samples into the histogram using a Gaussian

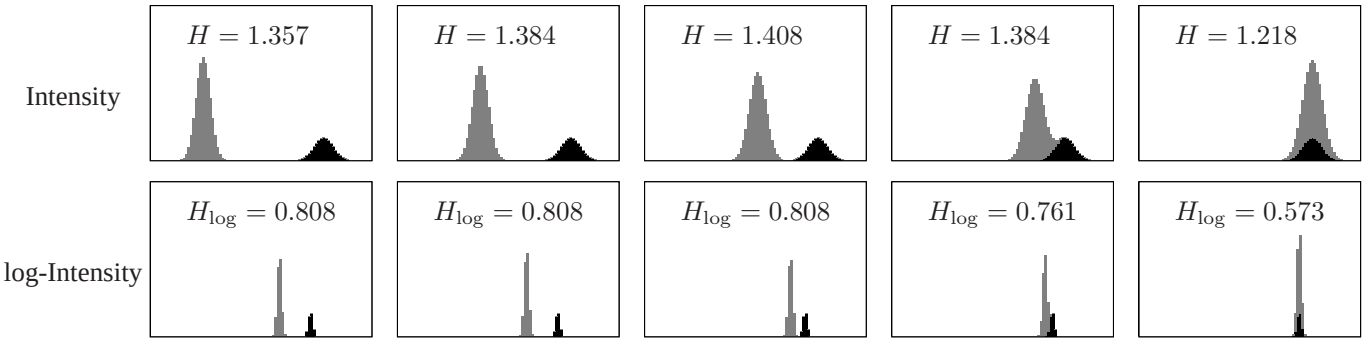

Fig. 1. Stacked histograms that illustrate the overlap of two Gaussian distributions: one (black) with fixed mean and standard deviation, and the other (gray) with increasingly scaled mean and standard deviation. The fixed distribution could represent intensities near the image center, which are mostly unaffected by vignetting, whereas the moving distribution could represent intensities at a larger distance, which are affected and thus darkened. *Top row:* Using intensity entropies, scaling the moving distribution, analogous to devignetting, widens and flattens this distribution as its constant number of samples is distributed over a wider range of values. The total entropy, H, thus increases until both distributions begin to overlap substantially. *Bottom row:* Entropy computation of the same two distributions as in the corresponding histograms in top row, but using log-intensities. The computed entropy values, $H_{\log}$, remain unchanged until the distributions begin to overlap, at which point the entropy begins to drop.

kernel. The discrete entropy is finally computed from the smoothed histogram as

$$H = \sum_k \hat{p}_k \log \hat{p}_k \tag{9}$$

where the discrete probability for each bin is

$$\hat{p}_k = \hat{n}_k / \sum_j \hat{n}_j. \tag{10}$$

C. Constrained Parametric Vignetting Model

One simple parametric function to describe lateral intensity drop-off due to vignetting is a sixth-order radial polynomial [2]. In this work, we use such a parametrization, but out of computational considerations model the inverse of the vignetting function, which we refer to as the gain function. Specifically, for a pixel index (x, y), let the gain function be

$$g_{a,b,c}(r) = 1 + ar^2 + br^4 + cr^6, \tag{11}$$

where

$$r = \frac{\sqrt{(x-\bar{x})^2 + (y-\bar{y})^2}}{\sqrt{\bar{x}^2 + \bar{y}^2}} \tag{12}$$

is the normalized radius of (x, y), i.e., the Euclidean distance of (x, y) from the image center $(\bar{x}, \bar{y})$, divided by the image diagonal. Thus, $r = 0$ in the image center and $r = 1$ in each of the four corners. Note that this description of the parametric model does not incorporate a shift of the vignetting function center, which is convenient and reduces the number of degrees of freedom but is otherwise not required by the devignetting algorithm.

Given g, the corrected image luminance at (x, y) is computed as

$$L_{\text{corr}}(x, y) = L_{\text{orig}}(x, y) g_{a,b,c}(r). \tag{13}$$

Because of the physical properties of the vignetting effect, g must be monotonically increasing in r for $0 < r < 1$. The gain function g can, therefore, be constrained to have a strictly positive first-order derivative

$$dg/dr = 2ar + 4br^3 + 6cr^5 > 0 \tag{14}$$

in that interval. From $r > 0$, it follows that

$$a + 2br^2 + 3cr^4 > 0. \tag{15}$$

Furthermore, substitution of $r^2 = q$ yields

$$a + 2bq + 3cq^2 > 0. \tag{16}$$

The two solutions of the associated equation are

$$q_{+/-} = \frac{-2b \pm \sqrt{4b^2 - 12ac}}{6c}. \tag{17}$$

As the original polynomial, g, is a function of normalized radius, and thus only evaluated in the interval $[0, 1]$, the following criteria are necessary and sufficient for g to be monotonically increasing within that range:

$$\frac{dg}{dr}(x) > 0 \forall x \in (0, 1) \Longrightarrow C_1 \vee C_2 \vee C_3 \vee C_4 \vee C_5 \tag{18}$$

where

$$\begin{aligned}
C_1 &= (c \geq 0 \wedge 4b^2 - 12ac < 0),\\
C_2 &= (c \geq 0 \wedge 4b^2 - 12ac \geq 0 \wedge q_- \leq 0 \wedge q_+ \leq 0),\\
C_3 &= (c \geq 0 \wedge 4b^2 - 12ac \geq 0 \wedge q_- \geq 0 \wedge q_+ \geq 0),\\
C_4 &= (c < 0 \wedge q_- \leq 0 \wedge q_+ \geq 0),\\
C_5 &= (c < 0 \wedge q_- \geq 0 \wedge q_+ \leq 0).
\end{aligned}$$

Intuitively, these conditions ensure that the derivative of g is positive for $r = 0$ and $r = 1$ (by considering the sign of c) and has no zero-crossings between 0 and 1. In summary, this provides a constraint on a, b, c as any set of these parameters that does not satisfy at least one of the five conjunctions, C_1 through C_5, is not monotonically increasing in the interval $(0, 1)$ and can thus be rejected as physically implausible.

These constraints also motivate the advantage of using a gain function, Eq. (11), rather than a drop-off function

$$F_{a,b,c}(r) = 1 - ar^2 + br^4 + cr^6, \tag{19}$$

for which the corrected image luminance at (x, y) would be computed by division, rather than multiplication, as

$$L_{\text{corr}}(x, y) = L_{\text{orig}}(x, y) / F_{a,b,c}(r). \tag{20}$$

A physically plausible drop-off function must satisfy $F(r) > 0$ for $0 \leq r \leq 1$, which is not guaranteed by the monotonic constraint $dF/dr < 0$ alone. In other words, a drop-off function requires a constraint on the function itself and on its first-order derivative. A gain function, as shown above, requires a constraint only on the derivative, because $g(r) > 0$ follows from $g(0) = 1$ and the monotonic constraint $dg/dr > 0$ for $r \in (0, 1)$.

D. Determining Model Parameters

Using log-intensity entropy as a merit function and the parameters of the constrained parametric vignetting model as degrees of freedom, the task of devignetting has been transformed into a constrained optimization problem: find the parameters of the vignetting model that minimize the log-intensity entropy of the corrected image while satisfying the monotonic drop-off constraint.

Constrained nonlinear optimization is an important field of research in and of itself (see for example [14]). Nevertheless, for the purpose of this paper, we use a very simple yet effective optimization strategy: hill climbing with rejection of invalid solutions. In short, optimization starts with all three vignetting parameters set to zero. Each of the parameters is then independently increased and decreased by a certain delta and the log-intensity entropy criterion of the resulting corrected image is evaluated. Out of the six evaluations, the parameters of the one with the minimum entropy value are selected and the search continues from there as before. If no further improvement is possible, the parameter delta is decreased by a factor k with $0 < k < 1$, and the search continues. This is repeated until a minimum delta threshold is reached. In all examples shown in this paper, we use initial delta 2.0, final delta 1/256, and $k = 0.5$. The monotonic drop-off constraints are satisfied simply by testing the inequalities in Eq. (18) and rejecting those parameter combinations for which the constraint is violated.

This is admittedly a very basic optimization strategy, but it is important to keep in mind that better optimization strategies should only improve the results – produce better devignetting in shorter computation times. As we demonstrate below, however, even without complex nonlinear optimization, effective devignetting can be achieved with good computational performance.

III. Results

In this section, results of the proposed method are shown for semi-synthetic images with simulated vignetting (Section III-A) as well as actual image examples (Section III-B). All corrected images shown below were corrected by applying vignetting functions computed using entropy estimation with 256 histogram bins. The histograms were smoothed using a Gaussian kernel with standard deviation $\sigma = 2$ bins and cut-off radius 8 bins.

A. Synthetic Ground Truth

For testing the proposed devignetting algorithm, a semi-synthetic vignette-free ground truth image was constructed, to which artificial vignette was then applied. We chose construction of a synthetic ground-truth image over calibration using captures of an evenly lit homogeneous flat surface, because with the resources available to us, it is impossible to guarantee perpendicular orientation and even lighting. The ground truth image is based on an actual digital photography (Fig. 2, left) and represents a more realistic (and substantially more difficult) devignetting problem than a flat, evenly illuminated image.

It is important that the ground truth itself is vignette free, because it is otherwise impossible to distinguish between correction of the artificial vignette and correction of residual actual vignette. To remove vignette from the ground truth image, we exploited two properties of vignetting: the radial drop-off and the relatively low spatial frequency of the darkening field.

An original, digitally captured image with 3264×2448 pixels was partitioned into tiles of 50×50 pixels each. These tiles were then randomly permuted (Fig. 2, right). The resulting image, which is the vignette-free ground truth image, has the same color and intensity distribution as the original image, but due to the small size and random spatial arrangement of the tiles no more vignetting is present in the permuted image. This is because vignetting is a low-frequency spatial effect that is negligible within each tile, and by randomly permuting the tiles the radial drop-off was eliminated, whereas the overall image noise level and the texture within each tile were preserved.

Known vignetting was then applied to the vignette-free ground truth image. Results on images with four different simulated vignetting functions applied to them are shown in Fig. 3. The selected parameters were somewhat arbitrary but within a realistic range, based on our analysis of actual vignetted images. The first three simulated vignetting functions each used a single parameter of the parametrization, their relative values adjusted to produce approximately the same global intensity difference between vignetted and ground truth image. The fourth simulated vignetting function used a combination of all three polynomial parameters.

The proposed devignetting algorithm was applied to each of the simulated images in Fig. 3. For each image, the algorithm was run with different levels of image downsampling (powers of 2 from 1 to 32). Note that the downsampling factors are per image dimension, i.e., for a factor of 4 every 16th sample of the image was used. Downsampling was regular in x and y, not random, and no pixel averaging or smoothing was applied. All devignetting runs used the same algorithm settings other than downsampling.

For comparison, we have also implemented the radial gradient symmetry criterion by Zheng *et al.* [8] and applied it to the same data. As our main focus in this work is the log-intensity entropy criterion, we used the same parametric vignetting model and optimization strategy for evaluation of the gradient symmetry criterion.

After devignetting each restored image was compared with the ground truth via the root mean squared error (RMSE) of the corrected luminance images. Computation time (on a single Pentium 4 CPU at 2.26 GHz clock speed) was also

(a) (b)

Fig. 2. Generation of a realistic, vignette-free semi-synthetic digital photograph. (a) Original digital image, 3264×2448 pixels, acquired with Canon PowerShot SD850 IS at 11.8 mm $f/4$. (b) Random shuffle of 50×50 pixel tiles to produce a vignette-free image.

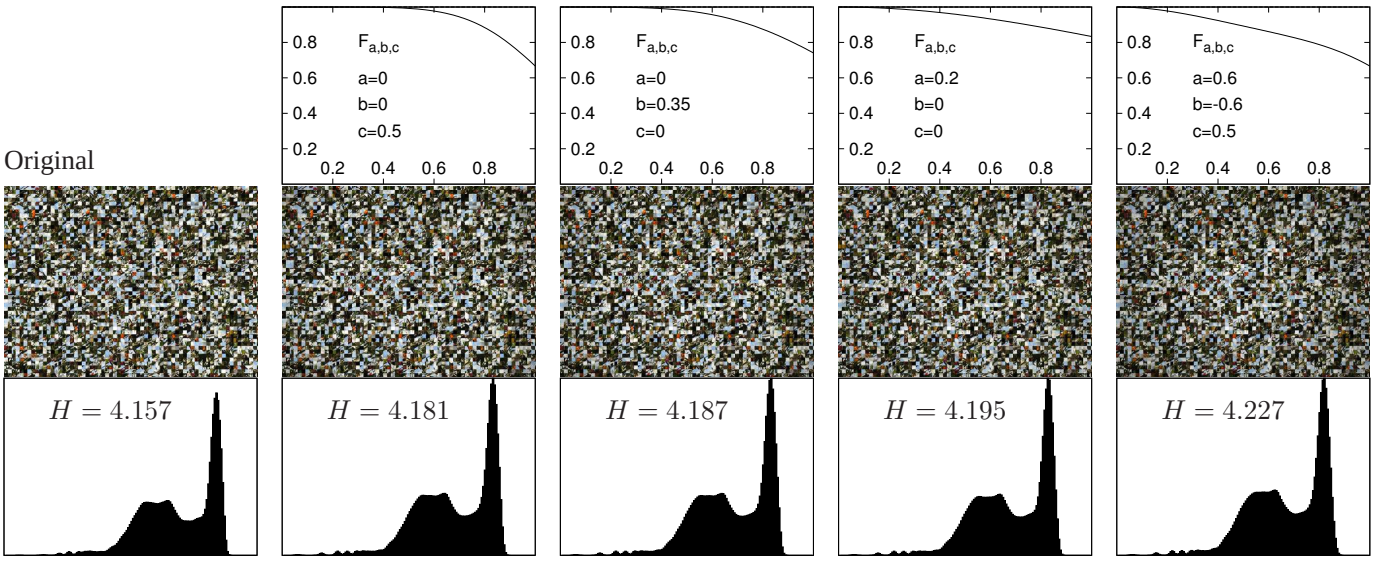

Fig. 3. Semi-synthetic test images with simulated vignetting, with corresponding histograms and log-intensity entropies. *Left column:* vignette-free ground truth image. *Remaining columns:* images with simulated vignetting using *a priori* parameters listed above each image. For the images with simulated vignetting the top row shows the simulated radial drop-off functions.

recorded for each devignetting run. All results are summarized in Table I. RMSE is used as the comparison metric, rather than the vignetting parameter values themselves, because parameter differences are not meaningful. Consider, for example, a redundant parametrization, $1+ar^2+br^2+cr^4+dr^6$, where the total weight of the square term can be arbitrarily distributed between the two coefficients a and b. The RMSE between corrected image and ground truth is unaffected by such effects.

For all test cases and for all downsampling factors, the entropy-based devignetting algorithm decreased the RMSE between the corrected and ground truth images by at least a factor of 5. Computation times depended greatly on the image downsampling, with typical times using full data with no downsampling around 20 s, but producing essentially identical devignetting accuracy with 1:8² downsampling in under 4 s per image.

The devignetting algorithm based on gradient symmetry, by comparison, used up to an order of magnitude more computation time, yet produced results with higher RMSE throughout the evaluation. More strikingly, gradient symmetry appears very sensitive to use of downsampled data, producing reliable results only when using full-resolution images. Entropy-based devignetting, on the other hand, showed hardly any worsening of the results when reducing image data by a factor of 32^2, bringing the necessary computation time to under a second in every case.

B. Real-World Examples

Results achieved using the entropy-based devignetting algorithm are shown in Fig. 4, all based on images captured on a

A Priori Parameters			RMSE		Devignetting with Downsampling Factor					
a	b	c	Uncorrected		full	1:2²	1:4²	1:8²	1:16²	1:32²
0	0	0.5	9.5	RMSE/Entropy	2.2	2.2	2.2	2.0	2.6	4.3
				Time	20.1 s	11.7 s	6.1 s	3.5 s	1.7 s	0.7 s
				RMSE/Gradient Symmetry	4.2	8.1	8.9	8.9	3.7	8.6
				Time	253.5 s	96.9 s	30.9 s	7.0 s	2.1 s	0.5 s
0	0.35	0	10.0	RMSE/Entropy	1.9	1.8	1.7	1.7	1.7	2.3
				Time	20.4 s	11.6 s	5.7 s	2.9 s	1.5 s	0.7 s
				RMSE/Gradient Symmetry	2.8	7.3	8.2	9.2	4.1	7.9
				Time	265.6 s	108.6 s	29.6 s	6.2 s	2.1 s	0.6 s
0.2	0	0	10.0	RMSE/Entropy	1.1	1.1	1.1	1.1	1.2	1.9
				Time	16.5 s	9.6 s	4.8 s	2.4 s	1.3 s	0.8 s
				RMSE/Gradient Symmetry	1.2	1.2	4.4	10.0	4.3	10.0
				Time	252.4 s	107.3 s	28.8 s	5.2 s	2.0 s	0.4 s
0.6	−0.6	0.5	19.5	RMSE/Entropy	3.9	3.9	3.9	3.9	4.0	4.4
				Time	17.2 s	9.7 s	4.9 s	2.4 s	1.3 s	0.7 s
				RMSE/Gradient Symmetry	4.1	4.5	4.4	16.1	19.5	17.5
				Time	289.0 s	125.8 s	36.9 s	7.7 s	1.2 s	0.4 s

TABLE I
TEST RESULTS USING SEMI-SYNTHETIC GROUND TRUTH IMAGE. ORIGINAL IMAGE SIZE: 3264×2448 PIXELS. ALL COMPUTATION TIMES WERE MEASURED ON A SINGLE PENTIUM 4 CPU AT 2.26 GHZ CLOCK SPEED.

Nikon D50 digital camera using a Nikkor 18–200 mm/3.5–5.6 zoom lens at varying focal lengths and apertures. We use our own, admittedly not representative, images for demonstration rather than obtaining images from public repositories, because to the best of our knowledge there is no such repository that provides high-quality (i.e., full resolution) unprocessed (e.g., not already devignetted) images. [1] Because the lack of a ground truth for these images prevents a quantitative comparison, we are also omitting the typically indistinguishable devignetting results for the gradient symmetry method for these images.

In all examples, our method estimated and corrected vignetting to produce visually convincing results (consider in particular the checkerboard composites of original and corrected images). Note the algorithm worked even on an image (Fig. 4, third row) that is virtually devoid of all but very small connected regions, i.e., the algorithm clearly does not depend on the existence of large areas to which the darkening function could be fitted. This comports with the results that demonstrate successful correction of simulated vignette on tiled images in Section III-A above.

An 11-picture panorama in Fig. 5 demonstrates the effectiveness of the proposed algorithm for image stitching. It also demonstrates qualitatively via line profile plots that the results using entropy-based and gradient symmetry-based devignetting are virtually identical.

As stated above, there are many algorithms for vignette correction that make use of the joint information in overlapping images, which would certainly perform at least as well as, and likely better than, the proposed algorithm in this application. However, the resulting panoramic image after devignetting provides additional, qualitative evidence that the proposed method is quite effective.

C. Non-radial Exposure Correction

The applicability of the proposed vignette correction method to correct local exposure more generally is demonstrated in Fig. 6, wherein vignetting correction using the radial polynomial model is compared with correction using a Cartesian polynomial model (6th order polynomials) that is directly analogous to the one used in Ref. [10].

While we can no longer refer to this processing as "correction," as it does not model an actual physical artifact, we note that the result of this processing could be considered more perceptually pleasing as it brightens the image foreground in the bottom third of the image frame. We note that this result could not have been achieved using the method by Zheng *et al.* [8], because the correction model is no longer radial and thus not tractable via radial gradient distributions[2].

IV. DISCUSSION

This paper has introduced a new algorithm for single-image devignetting based on constrained minimization of log-intensity entropy. The new method is extremely simple to implement and computationally efficient. It avoids fitting of drop-off functions to homogeneous image regions and thus requires no image segmentation. Indeed, we have demonstrated the

[1] Note to reviewers: we will provide all images from this paper in full, original resolution upon acceptance of this paper as supplemental data (most are already included as additional data in the paper submission to facilitate the reviewing process). We will also release all source code under the GPL to enable reproduction of our results and comparison with other methods.

[2] A closely related method [15], which lifts the radial constraint, has recently been proposed for MR bias field correction, but as this method uses image gradient sparseness, rather than radial gradient symmetry, it is arguably a different method, and as such has not been applied to image vignetting correction.

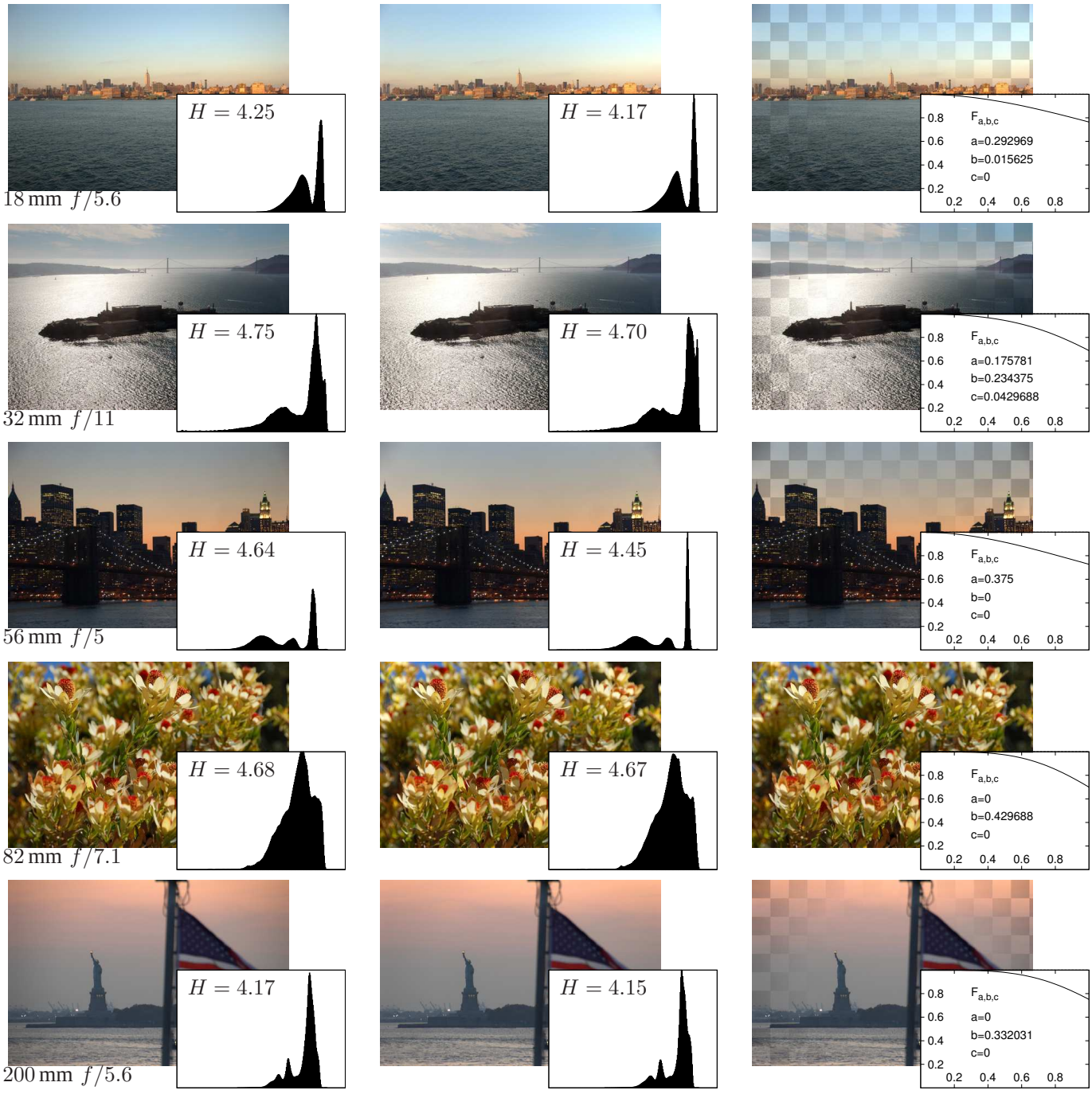

Fig. 4. Example images captured using a Nikon D50 camera with Nikkor 18–200 mm/3.5–5.6 lens. Focal length and aperture are given with each image. *Left:* Original images with focal length, aperture, original brightness histogram, and original log-intensity image entropy. *Right:* Corrected images with estimated drop-off function ($F = 1/g_{a,b,c}$ plotted vs. r), corrected brightness histogram, and corrected log-intensity image entropy. All histogram pairs for original and corrected images use identical y axis scales.

(a) Uncorrected

(b) Gradient Symmetry

(c) log-Intensity Entropy

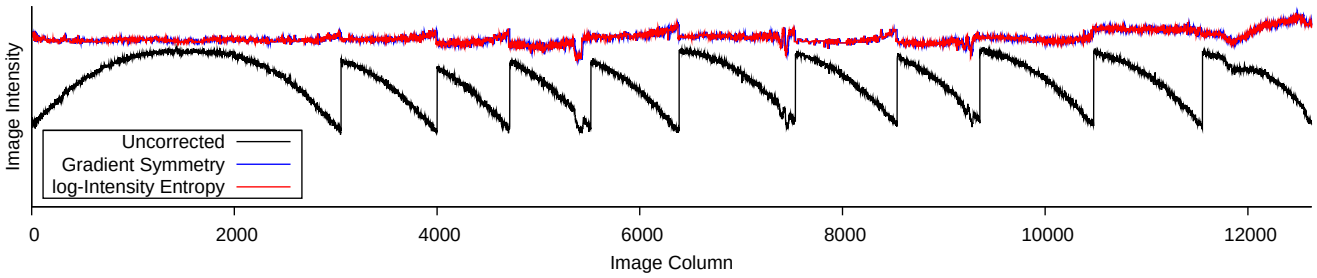

(d) Mosaic Line Profiles

Fig. 5. Proposed devignetting method applied to mosaicing 11 pictures. No blending or additional photometric corrections other than spatial distortion correction were applied. (a) Mosaic of uncorrected images as captured, (b) Mosaic after devignetting using gradient symmetry. (c) Mosaic after devignetting using entropy minimization. (d) Comparison plot of intensity profiles along the same horizontal line at the top of the image panorama. The profiles for the two devignetting methods are virtually indistinguishable.

method herein on images that defy segmentation into extended connected regions. Our method also decouples the parametric drop-off model from the optimization target function, and thus is applicable to exposure correction using non-radial drop-off models.

In a quantitative comparison of our method with a state-of-the art published algorithm [8] we have demonstrated our technique to be up to an order of magnitude faster, yet at least as accurate and substantially more robust to image data downsampling. In a qualitative comparison of both methods for image mosaicing both produced near-identical results when run on full-resolution image data.

While our comparison can be criticized for using the same vignetting model and optimization for the gradient symmetry criterion as for the entropy criterion, we note that this type of comparison is well established. For example, in image registration similarity measure, transformation model, optimization strategy are commonly treated as building blocks and evaluated orthogonal to one another. Furthermore, in our evaluation the simulated vignettes used the same parametric model as the devignetting algorithm, which means that we cannot make a valid comparison of different such models.

The quantitative evaluation using semi-synthetic ground truth images and simulated vignetting could be criticized also because the vignetting-free shuffled-blocks ground truth image (Fig. 2(b)) appear unrealistic. This objection is unfounded,

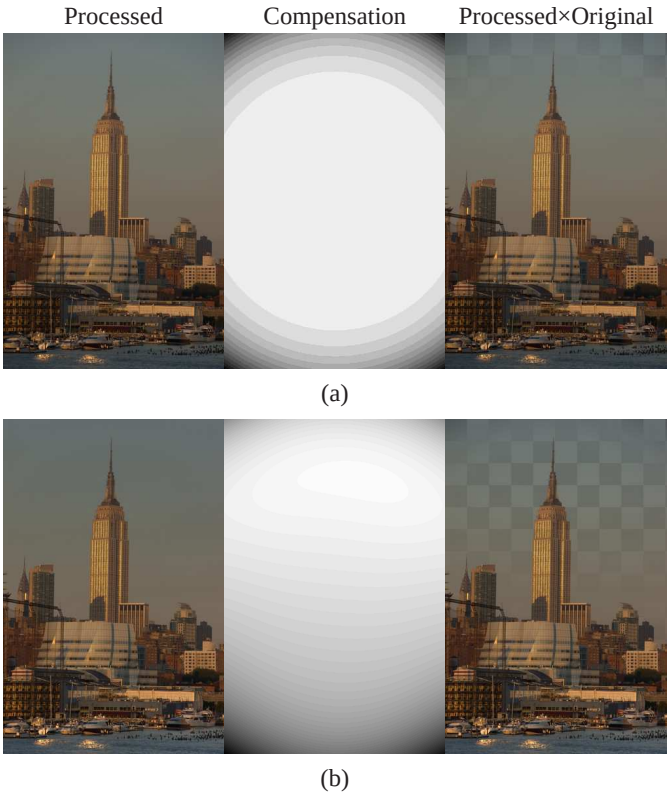

Fig. 6. Example of vignetting correction using entropy minimization and radial vs. non-radial drop-off model. *From left to right:* processed images, estimated drop-off fields, and checkerboard composite of original and processed images. *(a)* Exposure corrected using radial (vignetting) drop-off model. *(b)* Exposure corrected using non-radial drop-off model. For presentation, the estimated exposure compensation fields in each case were scaled independently to cover the entire range from white to black.

however, because one could in fact print the shuffled image and re-capture the printout using a camera. The second issue is that the evaluation is biased because the simulated vignetting effect uses the exact same parametric model as is used by the devignetting algorithm. This observation is correct, but we note that the primary contribution of this paper is the log-intensity entropy criterion, not the specific third-order polynomial radial parametrization.

We have deliberately not demonstrated devignetting of an image of a flat, evenly illuminated surface. Such demonstration could serve one of two purposes. First, it could give a simple, intuitive visual example of a captured vs. a corrected image. However, beyond the mere illustration of the correction problem this would be a pointless exercise as devignetting is trivial for such images. Indeed, the capture itself in this case already represents the darkening field that one is trying to estimate, making the estimation trivial and uninteresting. Successful correction in this case would say nothing about the performance of the correction method on more complex images.

The second use of a flat surface image capture is to provide a ground truth for devignetting images captured with the same imaging system. For that, however, even small imperfections of the capture process would compromise the calibration procedure, leaving the resulting calibration in doubt. We note that few (if any) researchers apparently have the necessary equipment to perform a thorough calibration, as otherwise there would be no need for retrospective devignetting methods at all. The growing number of publications on the subject suggests otherwise.

In summary, the proposed algorithm is a simple yet effective and efficient, fully-automatic, interaction-free method for devignetting of single images without explicit calibration. The method has virtually no tunable parameters, as histogram parameters and optimization parameters are essentially predetermined, and the devignetting results are, in our experience, stable for even substantial downsampling of the image data.

REFERENCES

[1] S. F. Ray, *Applied Photographic Optics*, 3rd ed. Focal Press, Mar. 2002.

[2] P. d'Angelo, "Radiometric alignment and vignetting calibration," in *The 5th International Conference on Computer Vision Systems, Bielefeld, March 21 - 24, 2007*, G. Sagerer, Ed., 2007. [Online]. Available: http://biecoll.ub.uni-bielefeld.de/volltexte/2007/101/

[3] D. B. Goldman and J.-H. Chen, "Vignette and exposure calibration and compensation," in *Computer Vision, 2005. ICCV 2005. Tenth IEEE International Conference*, vol. 1, 2005, pp. 899–906.

[4] J. Jia and C.-K. Tang, "Tensor voting for image correction by global and local intensity alignment," *IEEE Trans. Pattern Anal. Machine Intell.*, vol. 27, no. 1, pp. 36–50, Jan. 2005.

[5] S. B. Kang and R. S. Weiss, "Can we calibrate a camera using an image of a flat, textureless Lambertian surface?" in *6th European Conference on Computer Vision Dublin, Ireland, June 26 July 1, 2000 Proceedings, Part II*, ser. LNCS, vol. 1843. London, UK: Springer-Verlag, 2000, pp. 640–653.

[6] W. Yu, "Practical anti-vignetting methods for digital cameras," *IEEE Trans. Consum. Electron.*, vol. 50, no. 4, pp. 975–983, Nov. 2004.

[7] Y. Zheng, S. Lin, C. Kambhamettu, J. Yu, and S. B. Kang, "Single-image vignetting correction," *IEEE Trans. Pattern Anal. Machine Intell.*, vol. 31, no. 12, pp. 2243–2256, Dec. 2009.

[8] Y. Zheng, J. Yu, S. B. Kang, S. Lin, and C. Kambhamettu, "Single-image vignetting correction using radial gradient symmetry," in *IEEE Conference on Computer Vision and Pattern Recognition, CVPR*, 2008, pp. 1–8.

[9] F. J. W.-M. Leong, M. Brady, and J. O. McGee, "Correction of uneven illumination (vignetting) in digital microscopy images," *J Clin. Pathol.*, vol. 56, no. 8, pp. 619–621, Aug. 2003.

[10] B. Likar, J. B. A. Maintz, M. A. Viergever, and F. Pernuš, "Retrospective shading correction based on entropy minimization," *J. Microsc.*, vol. 197, no. 3, pp. 285–295, Mar. 2000.

[11] T. M. Cover and J. A. Thomas, *Elements of Information Theory*, 2nd ed. Hoboken, NJ: Wiley-Interscience, Jul. 2006.

[12] W. M. Wells, III., W. E. L. Grimson, R. Kikinis, and F. A. Jolesz, "Adaptive segmentation of MRI data," *IEEE Trans. Med. Imag.*, vol. 15, no. 4, pp. 429–442, Aug. 1996.

[13] J. Beirlant, E. Dudewicz, L. Györfi, and E. C. van der Meulen, "Nonparametric entropy estimation: An overview," *Int. J. Math. Stat. Sci.*, vol. 6, no. 1, pp. 17–39, 1997.

[14] M. S. Bazaraa, H. D. Sherali, and C. M. Shetty, *Nonlinear Programming: Theory and Algorithms*, 3rd ed. Hoboken, NJ: Wiley, 2006.

[15] Y. Zheng, M. Grossman, S. P. Awate, and J. C. Gee, "Automatic correction of intensity nonuniformity from sparseness of gradient distribution in medical images," in *Medical Image Computing and Computer-Assisted Intervention – MICCAI 2009. 12th International Conference, London, UK, September 20-24, 2009, Proceedings, Part II*, ser. LNCS, vol. 5762. Berlin/Heidelberg: Springer-Verlag, 2009, pp. 852–859.